NUCL SCI TECH (2021) 32:50
https://doi.org/10.1007/s41365-021-00880-4

Activation and pumping characteristics of Ti–Zr–V films deposited on narrow tubes

Bang-Le Zhu[1] · **Xiao-Qin Ge**[1] · **Si-Hui Wang**[1] · **Wei Wei**[1] · **Yi-Gang Wang**[1] · **Gong-Fa Liu**[1] · **Yong Wang**[1]

Received: 6 February 2021 / Revised: 11 March 2021 / Accepted: 18 March 2021 / Published online: 18 May 2021

Abstract Non-evaporable getter (NEG) films are an integral part of many particle accelerators. These films provide conductance-free evenly distributed pumping, a low thermal outgassing rate, and a low photon-and electron-stimulated desorption. These characteristics make it an ideal solution for resolving the non-uniform pressure distribution in conductance-limited narrow vacuum tubes. In this study, ternary Ti–Zr–V films were deposited on Si substrates and Ag–Cu (Ag 0.085 wt%) tubes with an inner diameter of 22 mm. All Ti–Zr–V films were prepared from an alloy target using the same DC magnetron sputtering parameters. The compositions and corresponding chemical bonding states were analyzed by X-ray photoelectron spectroscopy after activation at different temperatures. The test particle Monte Carlo (TPMC) method was used to measure the sticking probability of the Ti–Zr–V film based on pressure readings during gas injection. The results indicate that activation commences at temperatures as low as 150 °C and Ti^0, Zr^0, and V^0 exist on the surface after annealing at 180 °C for 1 h. Ti–Zr–V films can be fully activated at 180 °C for 24 h. The CO sticking probability reaches 0.15, with a pumping capacity of 1 monolayer.

Keywords Non-evaporable getter (NEG) · Accelerator vacuum · TPMC · Activation temperature

1 Introduction

New generation diffraction-limited storage rings have a compact lattice combined with small magnet apertures owing to the small horizontal beam size [1, 2], resulting in much smaller vacuum chamber apertures [3]. The vacuum system design of the Hefei Advanced Light Source Facility (HALF) results in the reduction in size of the aperture to 22 mm. This induces a challenge for the vacuum system design, as traditional lumped pumps are unable to provide the required ultra-high vacuum. Such problems can be solved by coating the inner surface of the storage ring vacuum chamber and inserting devices with non-evaporable getter (NEG) films. NEG films not only provide in situ conductance-free pumping speeds but also reduce outgassing from the walls [4, 5]. Coating the vacuum chambers with NEG films was originally applied in CERN [6–8] and then widely used in many ultra-high vacuum facilities, especially for particle accelerators, such as MAX IV [9], LHC [10], SOLEIL [11], DIAMOND [12], and ESRF [13].

Transition metals and their alloys are considered as ideal getter materials, and widely used getter materials are normally composed of Ti, Zr, and V. Ti and Zr have a good oxygen affinity and solubility, and V has a good oxygen diffusion property, which ensures maximum pumping

---

This work was supported by the National Natural Science Foundation of China (Nos. 11975226, 11905219), the Fundamental Research Funds for the Central Universities (No. WK2310000071) and the National Key Research and Development Program of China (2016YFA0402004).

✉ Bang-Le Zhu
zhubl@mail.ustc.edu.cn

Si-Hui Wang
sihui@ustc.edu.cn

Yong Wang
ywang@ustc.edu.cn

[1] National Synchrotron Radiation Laboratory, University of Science and Technology of China, Hefei 230029, China

performance and good activation characteristics [14]. NEG films are able to capture residual gases by impinging on their active surfaces to achieve ultra-high vacuum. However, NEG films are easily oxidized in ambient air. As a result, an inert oxide layer is generated on the surface, preventing residual gases from reacting with it further [15]. Therefore, NEG films need to be baked in a high vacuum to restore their sticking ability. This process is called activation, during which the oxides on the surface diffuse into the films, and new active metal surfaces reappear. The vacuum chambers of an accelerator are usually made of stainless steel, aluminum, oxygen-free copper, chromium zirconium copper, and silver copper. The high activation temperatures of NEG films do not only reduce the yield strength of vacuum system materials but also increase the cost of accelerator chambers, which are several hundred meters long. Many studies have been conducted on reducing the activation temperature of NEG films [16, 17]. Previous studies have shown that amorphous or nanocrystalline NEG coatings with a grain size of less than 100 nm have a lower activation temperature and better activation performance.

The activation temperature and vacuum performance of Ti–Zr–V getter films were investigated in this study for application of Ti–Zr–V getter films in the vacuum system of HALF. All Ti–Zr–V films were deposited by DC magnetron sputtering. The surface topography and thickness were assessed by scanning electron microscopy (SEM). The chemical state evolution on the surface of the film upon annealing was analyzed by X-ray photoelectron spectroscopy (XPS). The TPMC model was built and run to analyze the relationship between the measured pressure ratio and the NEG coating sticking probability using the MOLFLOW program.

2 Experimental procedures

Ti–Zr–V films were deposited on Si substrates and Ag–Cu (Ag 0.085 wt%) tubes with an inner diameter of 22 mm by DC magnetron sputtering. The cathode target was a ternary Ti–Zr–V alloy wire with a chemical composition equal to the atomic ratio. Before deposition, the Si substrates were first ultrasonically rinsed in acetone and then in absolute ethyl alcohol for 10 min. Finally, the obtained substrates were cleaned with deionized water and then dried using blowing nitrogen. The Ag–Cu tube was carefully cleaned by dipping in an alkaline solution and subsequent acid etching for 10 min. Then, the Ag–Cu tube was passivated by citric acid and finally dried using blowing nitrogen. The base pressure in the deposition facility was 1 $\times 10^{-5}$ Pa. The films were deposited using the pulsed unipolar current mode with a constant current of 0.1 A and a pulsed frequency of 40 kHz. The magnetic field strength used for the deposition was 200 G. Kr was supplied as sputtering gas because of its high sputtering yield, and the working pressure in the present study was 1 Pa.

The surface and cross-sectional morphologies of the Ti–Zr–V films were characterized using a Gemini SEM 500 Schottky field emission scanning electron microscope. The SEM was equipped with an Oxford Aztec series X-ray energy spectrometer (EDS) for characterizing the elemental distribution. The coated Si substrates were fractured to expose the new film flakes which were used to acquire cross-sectional SEM images. The thicknesses of the NEG films were determined using the cross-sectional images. The structure and crystallite sizes of the films were studied using X-ray diffraction (XRD). The grazing angle for the theta-theta rotating anode X-ray diffractometer was 1° and the 2θ data was varied between 30° and 60° with a step size of 0.02°. The evolution of the chemical states on the top surface of the thin films was identified using a PHI 5000 Versaprobe III multifunctional scanning X-ray photoelectron spectroscope using monochromatic Al Ka (Mono Al Ka) as an excitation source with a chamber pressure of 6.7 $\times 10^{-8}$ Pa. The temperature of the four-dimensional sample holder was adjusted in the range of − 140 to 600 °C. The film was heated to pre-set temperatures (25 °C, 150 °C, 160 °C, 170 °C, 180 °C, and 200 °C) and maintained for 1 h before acquiring the spectra of each individual element. The binding energy was calibrated using the C 1*s* core level orbital with a binding energy of 284.8 eV. The spectra of Ti 2*p*, Zr 3*d*, and C 1*s* were individually obtained within their respective binding energy ranges. The spectra of V 2*p* and O 1*s* were obtained together in the binding energy range of 509–538 eV.

The dedicated system shown in Fig. 1 was designed and built to investigate the pumping properties of the NEG-

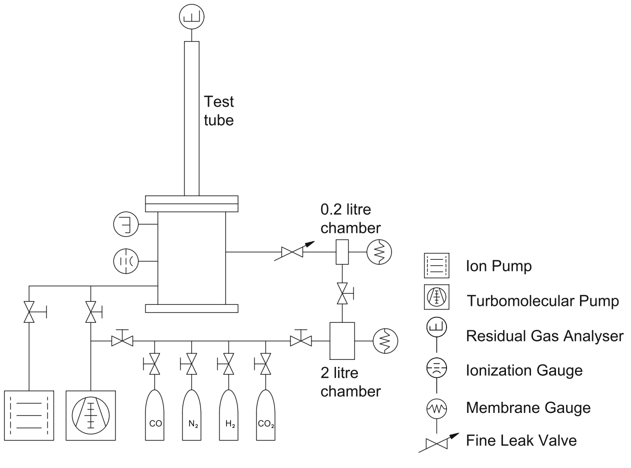

Fig. 1 Schematic of the vacuum system for analyzing vacuum properties of the tubular NEG tube

coated samples. The TPMC model was used to obtain an accurate evaluation of the sticking probability by reading the pressures at both ends during gas injection [18]. The TPMC model was built and run for each configuration using the MOLFLOW program written by Kersevan [19].

The main vacuum chamber comprised a tube with a diameter of 150 mm and a length of 200 mm, on the wall of which four holes with equal diameters of 35 mm were machined for gas injection, a residual gas analyzer (RGA), an ionization gauge and a valve connected to the pump assembly. The total pressure in the main chamber was measured using a calibrated ionization gauge, while the partial pressure was measured by the RGA, which had been calibrated against the ionization gauge. The NEG film was coated onto a 22 mm inner diameter Ag–Cu tube with two 35 mm flanges. This testing system enables the measurement of the sticking probability between 10^{-4} and 1 and the main chamber pressure from 10^{-8} to 10^{-4} Pa during testing [20]. A 500 L/s turbomolecular pump backed with a Drytel fore-vacuum pump was used for bakeout, NEG film activation, and gauge degassing. To prevent activated NEG film poisoning, a 300 L/s sputter ion pump was used to remove thermally desorbed gases from the uncoated parts of the test vacuum chamber after NEG film activation. The pressure in the test chamber reached 10^{-8} Pa after the uncoated parts of the system had been baked at 250 °C for 24 h. The new bakeout and activation processes described in Ref. [20] were carefully performed in this study.

The gas injection system consisted of two expansion vacuum chambers (volumes of 0.2 L and 2 L), an injection line connected to gas cylinders, and a pumping system consisting of a 75 L/s turbomolecular pump and a 10 m^3/h scroll pump. The injected gas flux was calculated with the pressure in the small expansion vacuum chamber (measured by a 0.1 Pa full-scale PREIFFER membrane gauge) during gas injection.

The test system was baked, and the tube coated with NEG film was activated. The injection system was pumped with a molecular pump and then filled with CO until the pressure in the smaller expansion chamber reached $\sim$ 5 Pa. The fine leak valve was opened after the test system had been cooled to 20 °C. The partial pressures of CO at both ends were recorded at the same time until the point at which the values at both ends were equal. The initial sticking probability of the NEG film was determined from the measured maximum pressure ratio using the TPMC method [18].

3 Results and discussion

3.1 Surface morphology and microstructure

The surfaces and cross-sectional morphologies of the Ti–Zr–V films are shown in Fig. 2). The surface morphologies (Fig. 2a) of the Ti–Zr–V film deposited onto the Si substrate exhibit uniform nanostructures, and a large number of nucleations can be observed. The films composed of 30.1 at.% Ti, 31 at.% V, 27.4 at.% Zr and 11.5 at.% O were observed through elemental mapping analysis by EDS. The three metallic elements are evenly distributed on the surface of the film. Cross-sectional images (Fig. 2b) of the thin film present columnar grain structures with a film thickness of approximately 0.8 µm. Meanwhile, many pores are also observed among the columnar grain structures.

The microstructures of the films deposited on Si were studied using X-ray diffraction (XRD). The XRD data for the as-received Ti–Zr–V films are shown in Fig. 3. The only diffraction peak at $2\theta = 37.5°$ associated with the film has a rather broad width. According to this diffraction peak, the average grain size in the films, as calculated by Scherrer's equation, is 2.10 nm.

3.2 Surface chemical states and activation evaluation by XPS

The NEG films were exposed to ambient air after deposition. Oxygen atoms are prone to be absorbed by the NEG films. Therefore, the surfaces of the as-received NEG films were almost completely oxidized. To recover the pumping ability, NEG films need to be heated to a certain temperature in an ultrahigh vacuum. The binding energy spectra and the variations in chemical states of each individual element of the NEG films with increasing annealing temperature are presented in Fig. 4. The resolved spectra of the as-received NEG and those activated at 150 °C and 180 °C are shown in Fig. 5. This reveals the surface chemical states of the as-received films in the initial and in the completely activated states.

As for the as-received NEG films, the Ti element was fully oxidized, and appeared in its stable oxide state TiO_2. According to a previous study, the oxides of Ti in various valence states correspond to different peaks in the spectra of Ti 2*p*. The $2p_{3/2}$ peaks at binding energies of 458.7 eV, 456.1 eV, 454.8 eV and 454.3 eV are attributed to Ti^{4+}, Ti^{3+}, Ti^{2+} and metallic Ti^0, respectively. After analyzing the spectra, it was determined that the Ti atoms on the

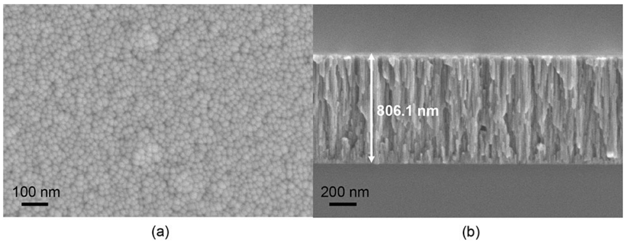

Fig. 2 Surface (**a**) and cross-sectional (**b**) images of Ti–Zr–V films

surface of the as-received NEG films were mainly consumed by TiO_2, and Ti_2O_3 occupied a marginal part. This is a typical characteristic of a natural oxide surface formed on Ti alloys [21].

As the NEG films are baked, it is obvious that the surface chemical states evolve drastically, as shown in the spectra (Fig. 4a). After being activated at 150 °C, the peaks in the Ti 2*p* spectra shifted toward lower binding energies and the corresponding FWMHs became wider compared with that of the as-received sample. When the annealing temperature was increased to 160 °C, the peaks in the spectrum shifted even further into the lower binding energy direction. Meanwhile, the $2p_{3/2}$ and $2p_{1/2}$ peaks are difficult to distinguish by simple visual inspection. As the activation temperature was further increased to 170 °C and finally to 180 °C, the peaks continued to shift toward the lower binding energy direction and became sharp again. The shift of the peak toward the direction of low energy indicates that the amount of Ti oxide begins to decrease [15]. The coexistence of TiO_2 and sub-oxides $TiO_x (0 < x < 4)$ causes wider FWMHs in the spectrum [22]. The above analysis indicates that Ti–Zr–V NEG films began to be activated at 150 °C, although the activation extent was rather limited. In addition, the amount of Ti oxides decreased with increasing annealing temperature. Considering that the samples were only annealed for 1 h, it is reasonable for the activation extent to increase and continue increasing with increasing holding time.

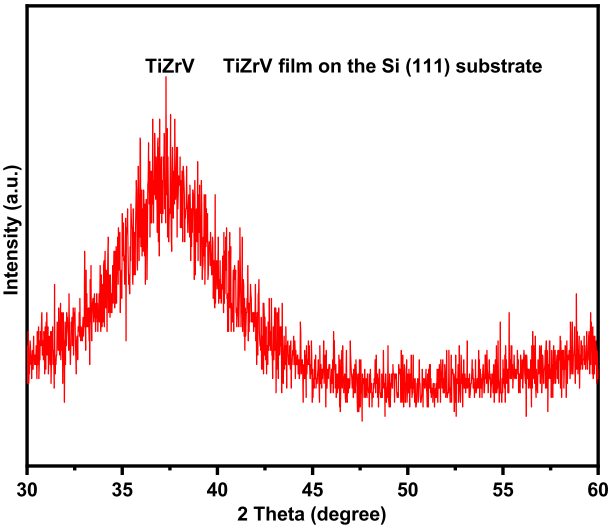

Fig. 3 XRD result for the as-received Ti–Zr–V film

The resolved spectrum of Ti 2*p* after annealing at 150 °C shows that it is mainly composed of TiO_2 and Ti_2O_3, whereas TiO cannot be identified (Fig. 5a). The amount of TiO_2 decreased, and the proportion of Ti_2O_3 increased as compared with the as-received sample. After activation at

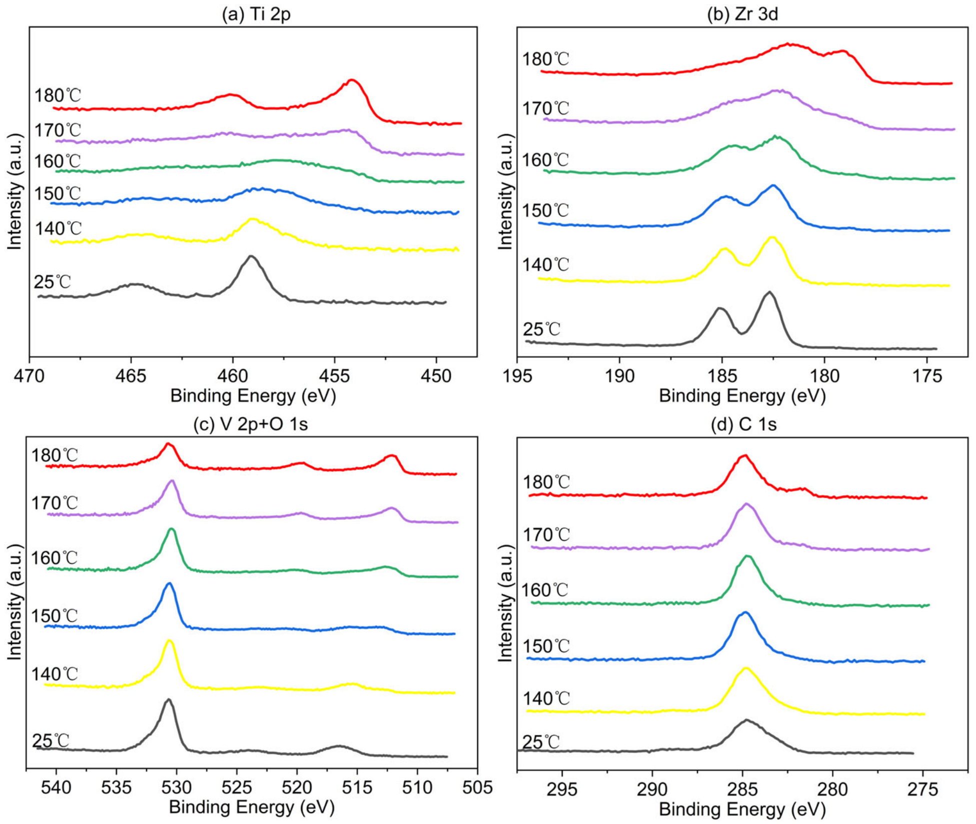

Fig. 4 (Color online) Evolution of XPS energy spectra of **a** Ti 2*p*, **b** Zr 3*d*, **c** V 2*p* + O 1*s* and **d** C 1*s* with an increase in annealing temperature

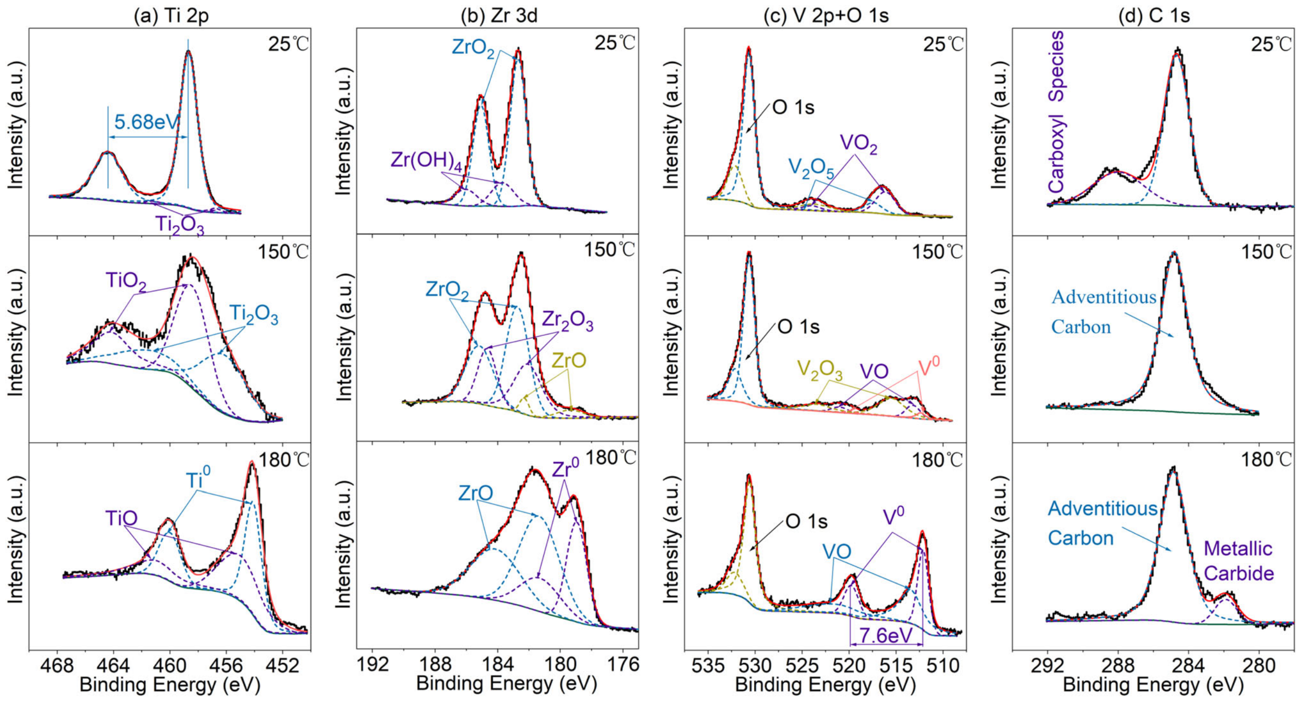

Fig. 5 (Color online) Resolved XPS energy spectra of **a** Ti 2*p*, **b** Zr 3*d*, **c** V 2*p* + O 1*s* and **d** C 1*s* tested at 25 °C (as-received), 150 °C and 180 °C

180 °C, a new peak at the binding energy of 454.3 eV could be resolved, indicating that the presence of metallic Ti and Ti atoms in the high-valence state are further reduced. At this time, only metallic Ti and TiO were present on the film surface.

In the as-received Ti–Zr–V film surface, Zr mainly existed in the form of ZrO_2. The binding energy of 182.5 eV corresponds to the Zr $3d_{5/2}$ peak. A peak at the binding energy of 183.7 eV is observed in the resolved spectrum, which can be attributed to the existence of zirconium hydroxides ($Zr(OH)_4$), as the Zr on the surface of the film readily reacts with O and H to form a passivation layer of oxides and hydroxides [23]. The resolved spectra (Fig. 5c) of O 1*s* also confirm this phenomenon, because in addition to a main peak at a binding energy of 530.6 eV, another peak at the binding energy of 532.1 eV can be observed, corresponding to metallic oxides and hydroxides, respectively [24, 25]. The coexistence of ZrO_2 and $Zr(OH)_4$ is a typical characteristic of Zr alloys exposed to ambient air.

The Zr 3*d* spectra of the samples annealed at various temperatures are shown in Fig. 4b. It is obvious that the peaks in the spectra shift toward the lower binding energy direction with an increase in annealing temperature, which is similar to the Ti spectra variation, indicating a reduction in zirconium oxides during the annealing process. This reduction was highly dependent on the annealing temperature. Specifically, for an annealing temperature of 140 °C, hardly any changes in the Zr 3*d* spectra could be observed as compared with that of the as-received sample. When the annealing temperature was increased to 150 °C, the positions of the Zr 3*d* peaks remained almost unchanged; nevertheless, the corresponding FWHMs of the peaks increased. Similar characteristics are also apparent for samples annealed at temperatures up to 170 °C. Moreover, the FWHMs of the Zr 3*d* spectra become wide enough that the two sub-peaks can hardly be distinguished. The increased FWHM of the Zr 3*d* spectra can be attributed to the coexistence of zirconium in various valence states. Upon further increasing of the temperature to 180 °C, the peaks clearly shifted and a bulge exists at the binding energy of 179 eV (representing metal Zr), indicating that metallic Zr already existed on the film surface.

The Zr spectra collected at various annealing temperatures were deconvoluted, and the results are shown in Fig. 5b. After activation at 150 °C, three peaks can be resolved, corresponding to ZrO_2, Zr_2O_3, and ZrO, respectively. Compared with the as-received sample, it was found that $Zr(OH)_4$ disappeared, the amount of TiO_2 decreased, and new ZrO and Zr_2O_3 components appeared. When activated at 180 °C, the main components of the film surface are ZrO and metallic Zr, and the remaining Zr oxides disappeared.

The V 2*p* + O 1*s* spectra of the as-received sample are shown in Fig. 5c. In contrast to Ti and Zr, which mainly exist in their highest oxide state, V_2O_5 is not the dominant form of V. Despite the constraints associated with the

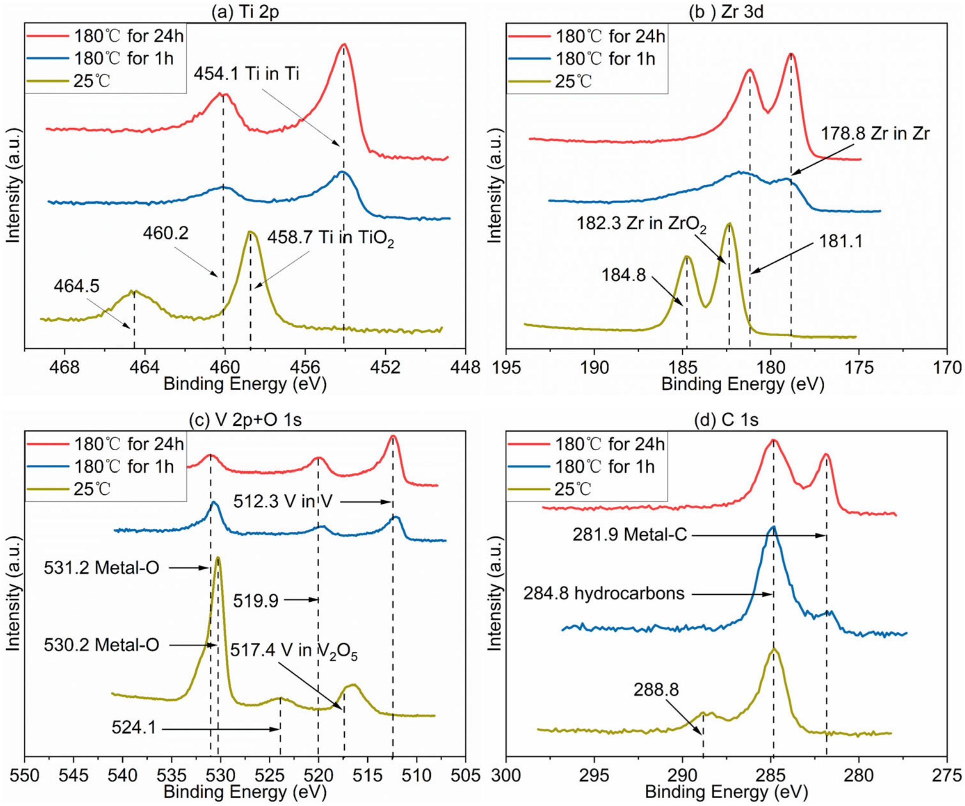

Fig. 6 (Color online) Comparison of XPS spectra of **a** Ti 2*p*, **b** Zr 3*d*, **c** V 2*p* + O 1*s* and **d** C 1*s* of the NEG film after activation at 180 °C for 0 (as-received), 1 h and 24 h

standard binding energy when resolving the spectra of V, a theoretical energy separation and 2:1 peak area relation for the $2p_{3/2}$ and $2p_{1/2}$ doublets were employed, however, the spectra of V $2p_{1/2}$ were still "underfitted," but the convergence of the $2p_{3/2}$ was quite good. Therefore, it is reasonable to analyze only the $2p_{3/2}$ portion [26].

Figure 4 shows that the evolution of the V 2*p* spectra is more rapid than that of Ti and Zr. After annealing at 150 °C, the spectrum greatly shifted toward a lower binding energy compared with that of the as-received sample, indicating that the vanadium oxides on the film surface evolved drastically. When the temperature was increased to 170 °C, the $2p_{3/2}$ peak of V in the spectrum increased significantly, which was almost the same for the sample annealed at 180 °C.

As shown in Fig. 5c, the binding energies at 517.4 eV and 516.1 eV correspond to the $2p_{3/2}$ orbitals of V_2O_5 and VO_2, respectively. After calculating the area below the two peaks, it was determined that the proportion of V_2O_5 is 33%, and the remainder is VO_2. V 2*p* spectra were also resolved for various annealing temperatures. When activated at 150 °C, V_2O_5 and VO_2 on the surface of the film completely disappeared, resulting in the coexistence of V_2O_3 and VO with metallic V. After increasing the temperature to 180 °C, the peak of V_2O_3 also disappeared, leaving only VO and metallic V on the surface of the NEG films.

As shown in Fig. 5d, it is obvious that a strong peak at a binding energy of 284.8 eV was present, corresponding to adventitious carbon on the film surface. Apart from the main peak, a broad peak at a binding energy of 288.8 eV can be attributed to carboxyl species on the getter surface [15]. When activated at a temperature higher than 170 °C, a small peak can be found at a binding energy of 281.9 eV, corresponding to metallic carbide.

The variations in the surface components of the NEG films after annealing at 180 °C for 24 h (the normally adopted activation time for engineering applications) were explored. The XPS spectra of the NEG films activated at 180 °C for 24 h are shown in Fig. 6. The amounts of titanium, zirconium, and vanadium on the surface of the Ti–Zr–V films greatly increased, while the proportion of oxygen greatly decreased. Compared with the sample activated at 180 °C for 1 h, the shapes of the corresponding peaks are much sharper, indicating that with an increase in activation time, the degree of reduction of metallic oxides on the surface of NEG films is higher, and correspondingly, the content of metallic components on the surface increases. The number of elemental metals on the surface increased. A comparison of the surface compositions of NEG films as determined by XPS in various states (as-received, annealed at 180 °C for 1 h and 24 h) is given in Table 1. It is obvious that the content of O decreased to

Table 1 Ratio of main elements as determined by XPS analysis for the NEG films of as-received, annealed at 180 °C for 1 h and 24 h

Elements	As-received (at.%)	180 °C for 1 h (at.%)	180 °C for 24 h (at.%)
O	52.7	21.1	10.3
Ti	5.3	6.2	11.8
Zr	9.2	11.3	17.1
V	5.3	6.4	11.9
C	27.5	55.0	48.9

10% after annealing at 180 °C for 24 h, indicating that the NEG films were almost fully activated.

3.3 Pumping properties by TPMC method

The pumping performance of the NEG films activated at 180 °C for 24 h was explored in this experiment. Figure 7 shows the partial pressure ratio at both ends of the tested NEG-coated tube (22 mm in diameter and 500 mm in length) as a function of the sticking probability of the NEG film. The initial sticking probability of the NEG film was acquired using the TPMC model with the assumption that the sticking probability is evenly distributed along the tested tube. The pumping capacity of the NEG film was calculated using the pressure in a smaller expansion vacuum chamber before and after gas injection, whereby one monolayer of CO was identified as 5.4×10^{14} molecules/cm^2. A pressure ratio of 10 between both ends of the tested tube was chosen as the saturation point of the NEG film. A maximum initial pressure ratio of 1000 was measured. The sticking probability of the coated Ti–Zr–V films was calculated to be 0.15, with a capacity of 1 monolayer.

Based on the above analysis, many pores exist in the boundaries of the columnar grains, which provide efficient diffusion paths for gases and can also be a container for storing gases. This can reduce the energy required for activation [14]. It can be concluded that the high-valence states (Ti^{4+}, Zr^{4+}, and $V^{5+} + V^{4+}$) of the three elements present a similar evolution process, changing from the highest valence state to the zero-valence state with an increase in the annealing temperature [27]. After annealing at 150 °C for 1 h, V^0 is present on the surface of the films, whereas Ti^0 and Zr^0 do not appear at this time, indicating that the reduction of vanadium oxides occurs first [24]. After heating to 180 °C for 1 h, Ti^0, Zr^0, and V^0 appear on the NEG film surface, indicating that NEG films can be completely activated by prolonging the activation time. The XPS spectra of the NEG film annealed at 180 °C for 24 h showed that the O ratio was only 10%, confirming that activation was completed. The results of the TPMC method show that the CO sticking probability reaches 0.15.

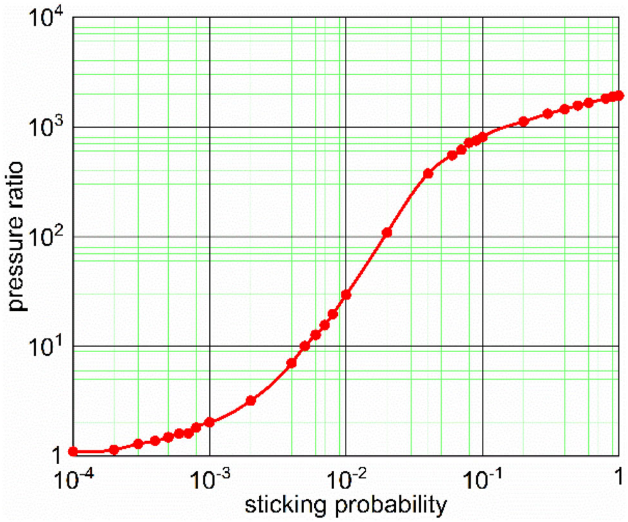

Fig. 7 (Color online) Pressure ratio as a function of the initial CO sticking probability of the NEG film for the 500 mm long tube with a diameter of 22 mm

4 Conclusion

Ti–Zr–V getter films were successfully deposited on the inner surface of an Ag-Cu pipe and a silicon substrate by DC magnetron sputtering. The evolution process of the NEG film components during activation at different annealing temperatures was detected by XPS, and the pumping speed and capacity were calculated using the TPMC method. The results show that the initial activation temperature of Ti–Zr–V films can be as low as 150 °C, and that Ti^0, Zr^0, and V^0 appear on the surface after annealing at 180 °C for 1 h. The Ti–Zr–V films showed a good pumping speed and capacity after annealing at 180 °C for 24 h. This provides an excellent solution for the vacuum system construction of the HALF.

Author Contributions All authors contributed to the study conception and design. Material preparation, data collection and analysis were performed by Bang-Le Zhu, Xiao-Qin Ge, Si-Hui Wang and Yong Wang. The first draft of the manuscript was written by Bang-Le Zhu and all authors commented on previous versions of the manuscript. All authors read and approved the final manuscript.

References

1. Z.B. Sun, L. Shang, F.L. Shang et al., Simulation study of longitudinal injection scheme for HALS with a higher harmonic cavity system. Nucl. Sci. Tech. **30**, 113 (2019). https://doi.org/10.1007/s41365-019-0627-x
2. D.C. Zhu, J.H. Yue, Y.F. Sui et al., Performance of beam size monitor based on Kirkpatrick–Baez mirror at SSRF. Nucl. Sci. Tech. **29**, 148 (2018). https://doi.org/10.1007/s41365-018-0477-y
3. P. He, Accelerator vacuum technology challenges for next generation synchrotron-light sources. In *Proceedings of the 8th International Particle Accelerator Conference*, IPAC2017, Copenhagen, Denmark, pp. 4830–4835 (2017). https://doi.org/10.18429/JACoW-IPAC2017-FRXAB1
4. V.V. Anashin, I.R. Collins, R.V. Dostovalov et al., Comparative study of photodesorption from TiZrV coated and uncoated stainless steel vacuum chambers. Vacuum **75**, 155–159 (2004). https://doi.org/10.1016/j.vacuum.2004.01.080
5. O.B. Malyshev, A.P. Smith, R. Valizadeh et al., Electron stimulated desorption from bare and nonevaporable getter coated stainless steels. J. Vac. Sci. Technol. A **28**, 1215–1225 (2010). https://doi.org/10.1116/1.3478672
6. C. Benvenuti, P. Chiggiato, P.C. Pinto et al., Vacuum properties of TiZrV non-evaporable getter films. Vacuum **60**, 57–65 (2001). https://doi.org/10.1016/S0042-207X(00)00246-3
7. C. Benvenuti, Non-evaporable getters: from pumping strips to thin film coatings. In: *6th European Particle Accelerator Conference, EPAC1998*, Stockholm, Sweden, pp. 200–204 (1998) https://accelconf.web.cern.ch/e98/PAPERS/THZ02A.PDF
8. C. Benvenuti, P. Chiggiato, A. Mongelluzzo et al., Influence of the elemental composition and crystal structure on the vacuum properties of Ti–Zr–V nonevaporable getter films. J. Vac. Sci. Technol. A **19**, 2925–2930 (2001). https://doi.org/10.1116/1.1414122
9. E. Al-Dmour, M.J. Grabski, The vacuum system of MAX IV storage rings: Installation and conditioning. In: *Proceedings of the 8th International Particle Accelerator Conference, IPAC2017*, Copenhagen, Denmark, pp. 3468–3470 (2017). https://doi.org/10.18429/JACoW-IPAC2017-WEPVA09
10. J.M. Jimenez, LHC: the world's largest vacuum systems being operated at CERN. Vacuum **84**, 2–7 (2009). https://doi.org/10.1016/j.vacuum.2009.05.015
11. C. Herbeaux, N. Bèchu, A. Conte, et al., Vacuum conditioning of the SOLEIL storage ring with extensive use of NEG coating. In: *11th European Particle Accelerator Conference, EPAC2008*, Genoa, Italy, pp. 3696–3698 (2008) https://accelconf.web.cern.ch/e08/papers/thpp142.pdf
12. O.B. Malyshev, M.P. Cox, Design modelling and measured performance of the vacuum system of the diamond light source storage ring. Vacuum **86**, 1692–1696 (2012). https://doi.org/10.1016/j.vacuum.2012.03.015
13. M. Hahn, Operational experience and relation to deposition process for NEG-coated chambers installed on the ESRF electron storage ring. Vacuum **81**, 759–761 (2007). https://doi.org/10.1016/j.vacuum.2005.11.051
14. O.B. Malyshev, *Vacuum in Particle Accelerators: Modelling, Design and Operation of Beam Vacuum Systems* (Wiley, Hoboken, 2020).
15. Z. Abboud, O. Moutanabbir, Temperature-dependent in situ studies of volatile molecule trapping in low-temperature-activated Zr alloy-based getters. J. Phys. Chem. C **121**, 3381–3396 (2017). https://doi.org/10.1021/acs.jpcc.6b11426
16. A.E. Prodromides, C. Scheuerlein, M. Taborelli, Lowering the activation temperature of TiZrV non-evaporable getter films. Vacuum **60**, 35–41 (2001). https://doi.org/10.1016/S0042-207X(00)00243-8
17. C. Benvenuti, J.M. Cazeneuve, P. Chiggiato et al., A novel route to extreme vacua: the non-evaporable getter thin film coatings. Vacuum **53**, 219–225 (1999). https://doi.org/10.1016/S0042-207X(98)00377-7
18. O.B. Malyshev, K.J. Middleman, Test particle Monte-Carlo modelling of installations for NEG film pumping properties evaluation. Vacuum **83**, 976–979 (2009). https://doi.org/10.1016/j.vacuum.2008.11.008
19. R. Kersevan, J.L. Pons, Introduction to MOLFLOW+: new graphical processing unit-based Monte Carlo code for simulating molecular flows and for calculating angular coefficients in the compute unified device architecture environment. J. Vac. Sci. Technol. A **27**, 1017–1023 (2009). https://doi.org/10.1116/1.3153280
20. O.B. Malyshev, K.J. Middleman, J.S. Colligon et al., Activation and measurement of nonevaporable getter films. J. Vac. Sci. Technol. A **27**, 321–327 (2009). https://doi.org/10.1116/1.3081969
21. C. Sittig, M. Textor, N.D. Spencer et al., Surface characterization of implant materials cp Ti, Ti–6Al–7Nb and Ti–6Al–4V with different pretreatments. J. Mater. Sci. Mater. Med. **10**, 35–46 (1999). https://doi.org/10.1023/A:1008840026907
22. C.J. Nelin, P.S. Bagus, M.A. Brown et al., Analysis of the broadening of X-ray photoelectron spectroscopy peaks for ionic crystals. Angew. Chem. Int. Ed. **50**, 10174–10177 (2011). https://doi.org/10.1002/anie.201100964
23. G. Lu, S.L. Bernasek, J. Schwartz, Oxidation of a polycrystalline titanium surface by oxygen and water. Surf. Sci. **458**, 80–90 (2000). https://doi.org/10.1016/S0039-6028(00)00420-9
24. S.H. Wang, Z.W. Wang, X. Shu et al., Activation characterization of the Ti–Zr–V getter films deposited by magnetron sputtering. Appl. Surf. Sci. **528**, 147059 (2020). https://doi.org/10.1016/j.apsusc.2020.147059
25. I. Fongkaew, R. Akrobetu, A. Sehirlioglu et al., Core-level binding energy shifts as a tool to study surface processes on $LaAlO_3/SrTiO_3$. J. Electron. Spectrosc. Relat. Phenom. **218**, 21–29 (2017). https://doi.org/10.1016/j.elspec.2017.05.009
26. M.C. Biesinger, L.W.M. Lau, A.R. Gerson et al., Resolving surface chemical states in XPS analysis of first row transition metals, oxides and hydroxides: Sc, Ti, V, Cu and Zn. Appl. Surf. Sci. **257**, 887–898 (2010). https://doi.org/10.1016/j.apsusc.2010.07.086
27. J. Zemek, P. Jiricek, XPS and He II photoelectron yield study of the activation process in Ti–Zr NEG films. Vacuum **71**, 329–333 (2003). https://doi.org/10.1016/S0042-207X(02)00760-1